

WORKSHOP ON STRUCTURAL DYNAMICS AND  
CONTROL INTERACTION OF FLEXIBLE STRUCTURES

National Aeronautics and  
Space Administration

George C. Marshall Space Flight Center  
Marshall Space Flight Center, Alabama 35812

L. P. Davis, J. F. Wilson  
Sperry Corporation  
Aerospace and Marine Group  
Phoenix, Arizona 85036

R. E. Jewell  
National Aeronautics and Space Administration  
George C. Marshall Space Flight Center  
Marshall Space Flight Center, Alabama 35812

April 22-24, 1986

**PRECEDING PAGE BLANK NOT FILMED**

## ABSTRACT

The Hubble Space Telescope features the most exacting line of sight jitter requirement thus far imposed on a spacecraft pointing system. Consideration of the fine pointing requirements prompted an attempt to isolate the telescope from the low level vibration disturbances generated by the attitude control system reaction wheels. The primary goal was to provide isolation from axial component of wheel disturbance without compromising the control system bandwidth. At Sperry Corporation, a passive isolation system employing metal springs in parallel with viscous fluid dampers was designed, fabricated, and space qualified. Stiffness and damping characteristics are deterministic, controlled independently, and have been demonstrated to remain constant over at least five orders of input disturbance magnitude. The damping remained purely viscous even at the data collection threshold of  $.16 \times 10^{-6}$  in input displacement, a level much lower than the anticipated Hubble Space Telescope disturbance amplitude. Vibration attenuation goals were obtained and ground test of the vehicle has demonstrated the isolators are transparent to the attitude control system.

## INTRODUCTION

The Hubble Space Telescope (HST), shown in Figure 1, provides an optical image for five scientific instruments and three Fine Guidance Sensors. The vehicle is approximately 44 feet long and weighs 24,000 pounds. It is designed for STS insertion into a circular orbit of 320 NM for a 15-year mission. On-orbit maintenance and new technology upgrades during the mission are anticipated. To preclude the possibility of contamination of the optical elements no chemical reaction propulsion systems are onboard. Attitude control is provided by the Reaction Wheel Assemblies (RWAs) and the magnetic momentum control system. Reboost following orbital decay will be provided by the orbiter.

## POINTING CONTROL SYSTEM

The primary elements of the Pointing Control System (PCS) used for fine pointing are the digital computer, reaction wheels, magnetic momentum system, rate gyro complement, and two of the Fine Guidance Sensors. Pointing torques are applied with the RWAs. The magnetic momentum system is used to desaturate the RWAs and minimize the wheel speed excursions. The four RWAs are positioned with their spin axes inclined at 20 degrees to the telescope optical axis as in Figure 2. Two RWAs provide torque along the pitch and roll axes and two provide torque along the yaw and roll axes. The array is thus redundant in that it can provide control at reduced capacity following the loss of any one RWA. Additional coarse pointing attitude information is available from fixed head star trackers and sun sensors. Finally, a backup control system with backup rate gyros is provided for increased mission reliability.

REPRINTED FROM VIBRATION DAMPING WORKSHOP, MARCH 6, 1986

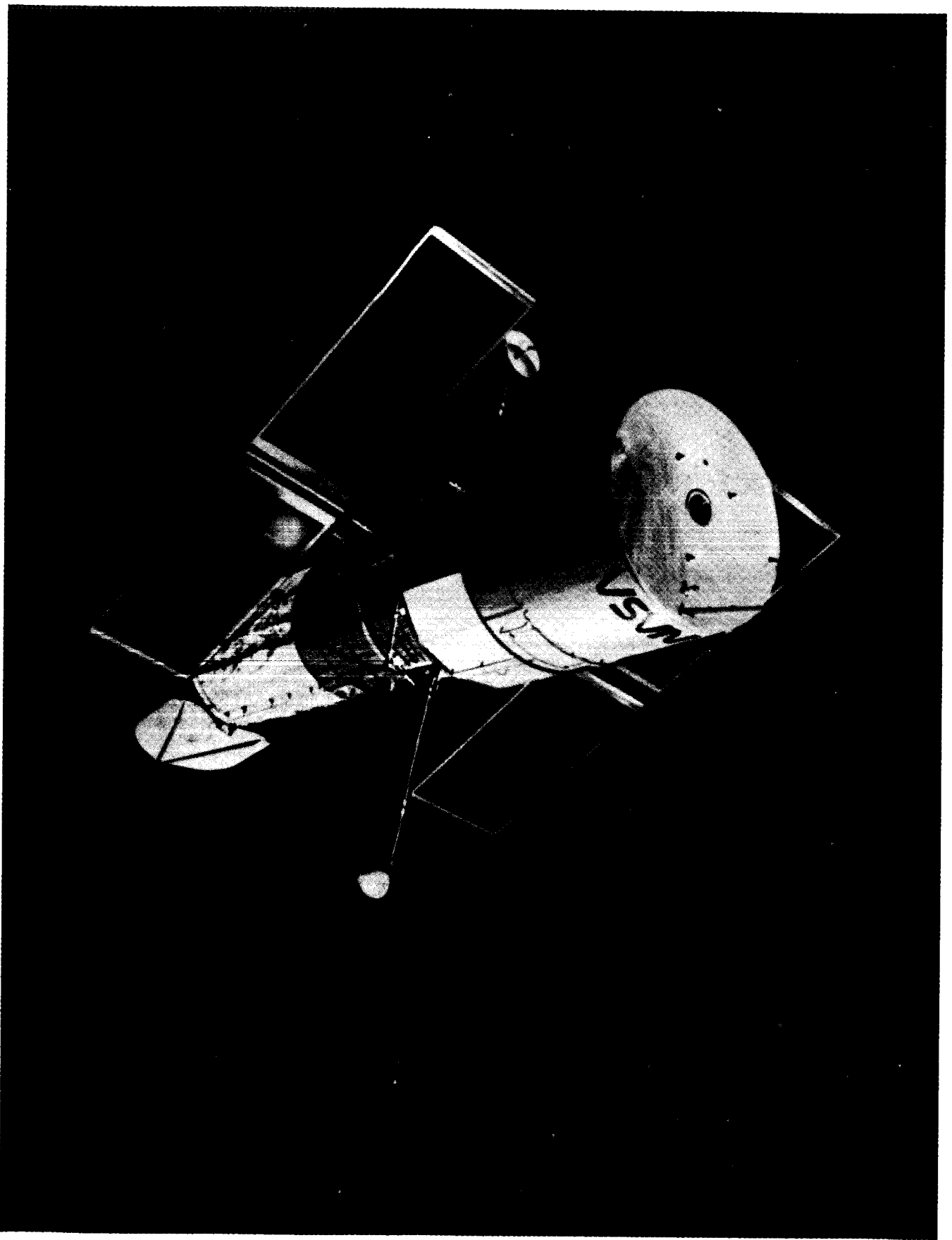


Figure 1

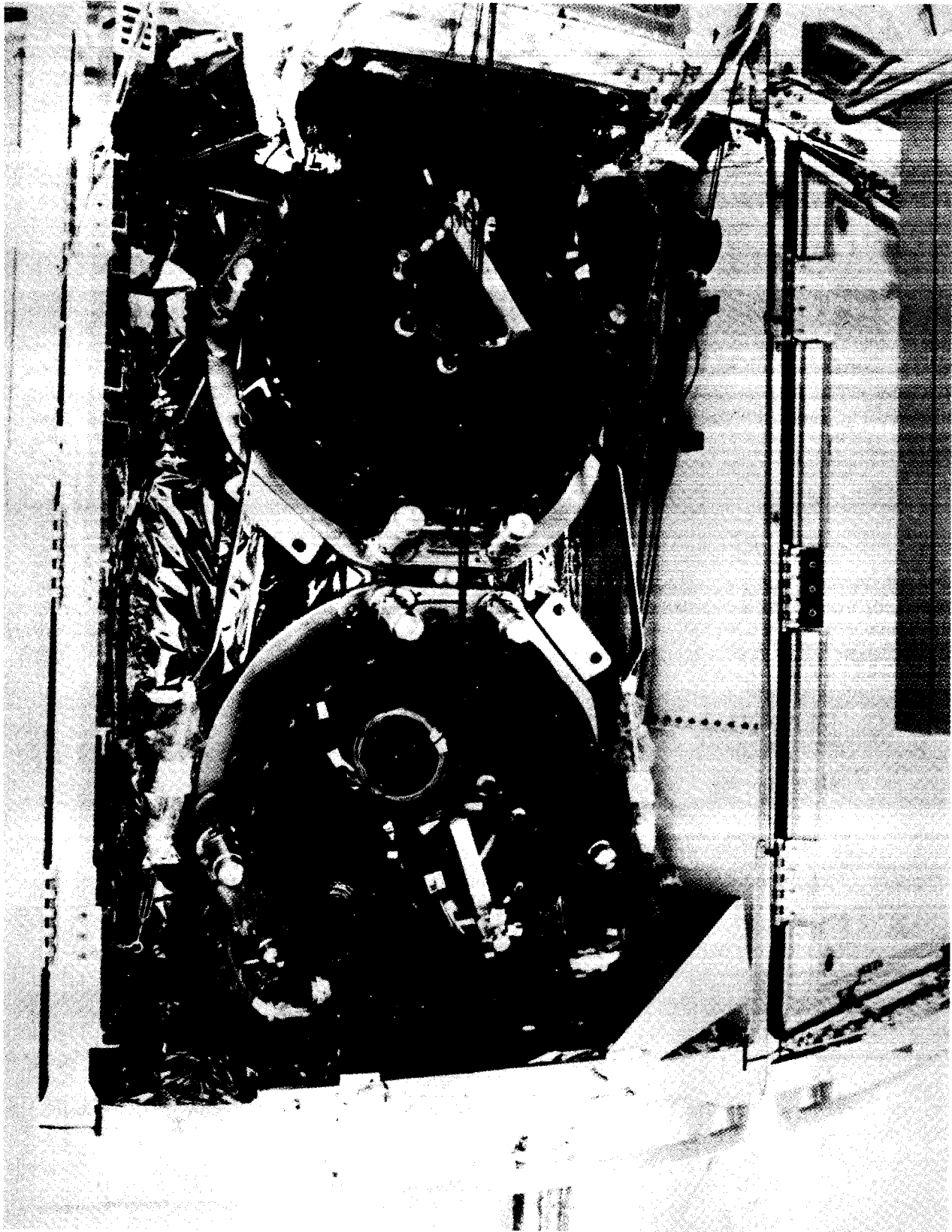


Figure 2

ORIGINAL PAGE IS  
OF POOR QUALITY

HST pointing accuracy and stability are defined in terms of Line Of Sight (LOS) error of the principal ray at the final imaging element, which includes the errors from all the optical elements in the path. Jitter predictions involve modeling of the disturbance sources, the HST structural transmissivities, and ray tracing between the various optical elements. The HST image stability requirement for periods up to 24 hours is .007 arcsec rms. This requirement is also to be maintained in any period as short as 10 seconds, which limits the averaging of short duration disturbances. The HST pointing repeatability requirement for periods up to 100 hours is .01 arcsec. Pointing performance of a satellite at these levels has not been previously obtained. LOS jitter sources include random sensor noise, coherent sources due to rotating machinery, thermal gradient effects, and residual transients due to recent large amplitude maneuvers. Since the RWAs are the most massive rotating machines onboard and must be operated continuously during science acquisition they received considerable attention in the jitter reduction effort. Jitter models indicated that the LOS was most sensitive to axial RWA disturbances owing to the vehicle configuration.

### REACTION WHEEL INDUCED VIBRATION

An RWA produces vibration disturbances when it rotates due to imperfections in the electromagnetics and their drive electronics, unbalance of the rotor, and imperfections in the spin bearings. In the case of the HST RWA, the electromagnetics and electronics were designed to produce negligible disturbances relative to the latter sources. The rotors were balanced to the point that the unbalance was at least as small as and indistinguishable from disturbances due to geometric imperfections in the spin bearings. The bearing geometry disturbances occur at many harmonics of wheel speed, and balancing alters only the once per revolution harmonic, so further improvements in balance are unproductive. The bearing geometry disturbances were minimized through the use of bearings with nearly perfect geometry (equivalent of ABEC 9) and by selectively matching the bearings for lowest net disturbance. This procedure is thought to result in state-of-the-art vibration reduction.

Some of the lower frequency first order disturbances are shown in Figure 3. These are the maximum, average, and minimum force levels for the five flight RWAs and the engineering unit while running at 1500 rpm. Also shown is a table summarizing the sources of these harmonics. In the HST bearing the ball groups rotate .35 times as fast as the rotor so harmonics of 1.0, .35 and their difference occur.

In Figure 4 measured data is shown for the axial force at once per revolution as wheel speed is varied from 0 to 3000 rpm. Also shown is the least square curve fit to the data based on the assumption that force is proportional to the square of wheel speed. A similar correlation with wheel speed squared is found for other harmonics at frequencies below the first resonance of the RWA and test fixture. This correlation suggests that at low frequency the disturbances have the form  $f = M\Delta(NW)^2$  where  $f$  is the disturbance force,  $M$  is the mass of the rotor,  $\Delta$  is the geometrical runout in the bearing,  $N$  is the harmonic number, and  $W$  is the wheel speed. Using this assumption,  $\Delta$  for each harmonic may be determined in the least square sense. This was done for the flight units and is tabulated in Figure 4. Since the predicted geometry errors are within the bearing specification and are not practically measurable this model of the bearing disturbance was accepted.

**BALL BEARING DISTURBANCES**

- 0.35 HARMONIC (BALL RETAINER)
- 1.0 HARMONIC (MASS UNBALANCE)
- 2.0 HARMONIC (RACE TO RACE MISALIGNMENT)
- 2.8 HARMONIC (OUTER RACE DEFECTS)
- 5.2 HARMONIC (INNER RACE DEFECTS)
- 5.6 HARMONIC (OUTER RACE DEFECTS)

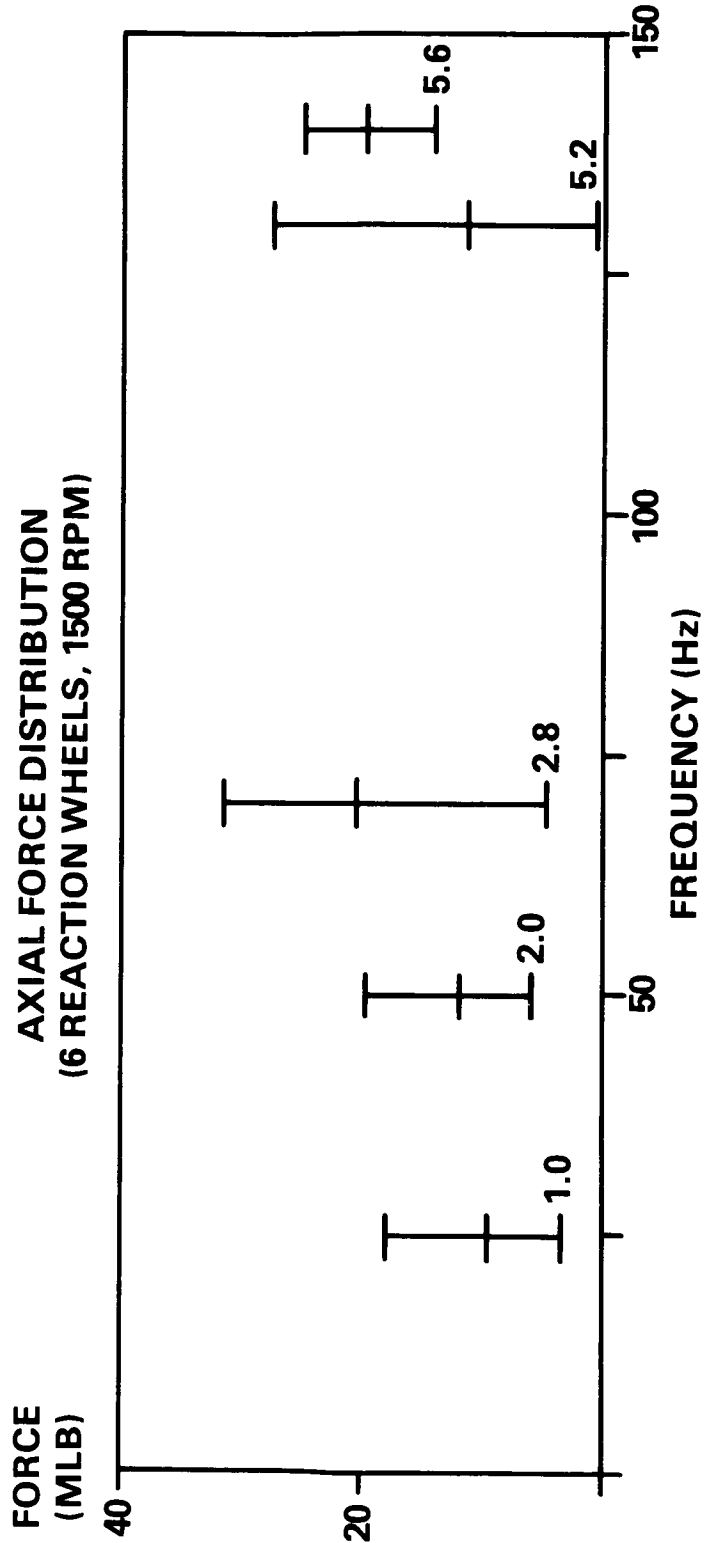


Figure 3

# 1g Hardmount Axial 1.0 Component

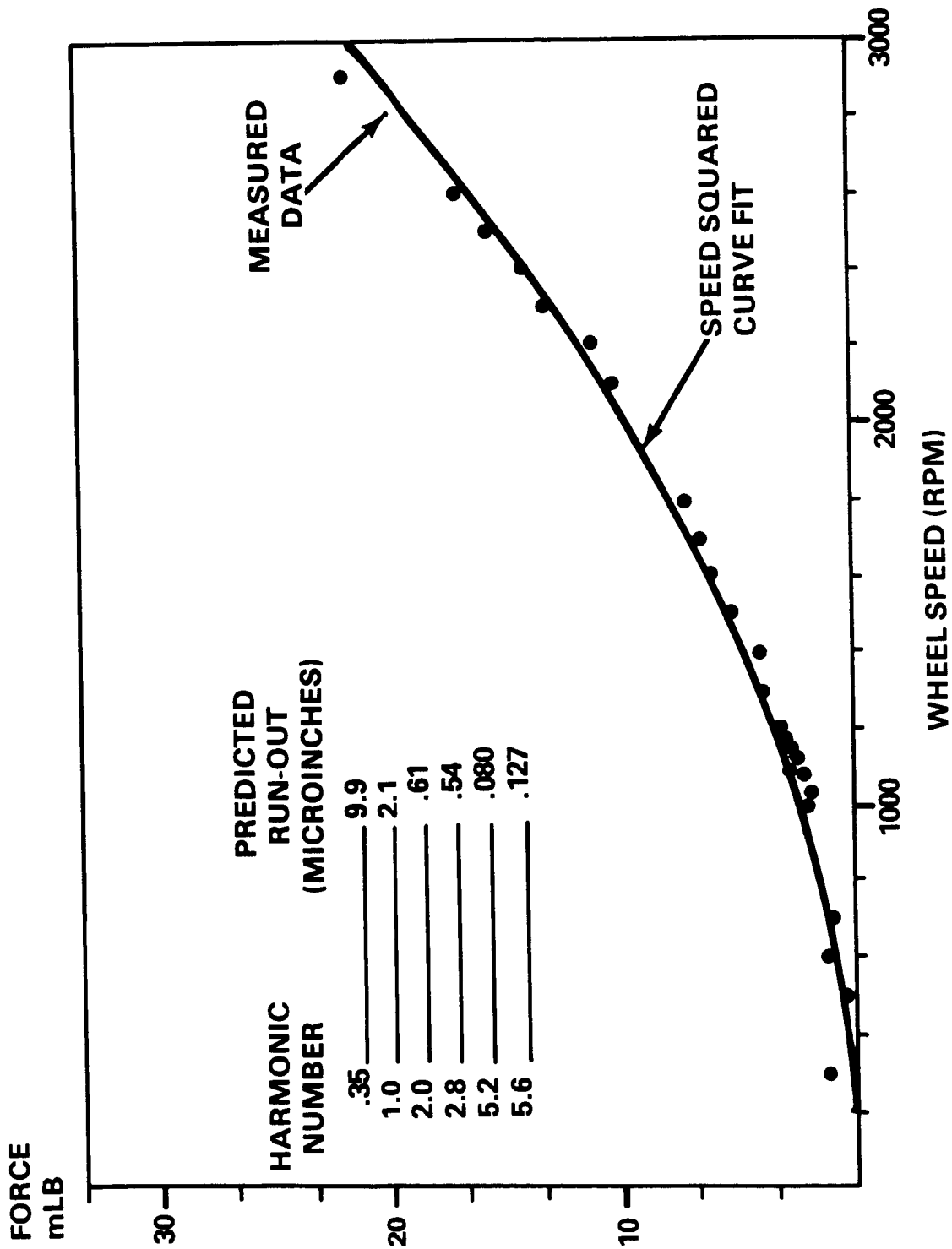


Figure 4

## VIBRATION ISOLATION SYSTEM

The nature of the RWA vibration disturbances is that there are many harmonics, sweeping a wide frequency range as wheel speed is run up and down, with amplitudes increasing as the square of speed. LOS jitter models predicted marginal performance due to axial disturbances at the higher wheel speeds above 10 Hz (600 RPM) so passive isolation of the RWAs was a logical approach. Initial evaluations were made with wire rope isolators. The PSD of acceleration response due to force input for this isolator is shown in Figure 5. The input force level was varied from .0045 to .750 pound. The transfer function is nonlinear in stiffness and damping as a function of disturbance amplitude. Both these tendencies are explained to the first order by the loss of sliding friction in the wire rope as the amplitude is reduced. These nonlinearities make accurate modeling of the isolator very difficult. An additional drawback is the lack of strict determinism in the design of the stiffness and damping properties since these characteristics cannot be independently controlled.

These difficulties led to the development of the viscous fluid damped isolator shown in Figure 6. A simplified schematic and a cutaway of the flight design are shown. In the dual chamber schematic damping fluid is contained by two metal bellows supporting the center isolated portion. When the center portion moves axially fluid must flow from one bellows chamber to the other, incurring viscous losses as it flows. The damping value is determined by the viscosity of the fluid and the dimensions of the annular passage between the chambers. The stiffness is determined by the bellows design. These characteristics are deterministic and independent. For radial motion the stiffness is also deterministic although the damping is less so due to the complex flow. The flight design works on the same principal but acquired additional complexity. Coil springs were added in parallel with the bellows which effectively determine the spring rates. A third preloaded bellows chamber was added outboard to accommodate thermal expansion of the fluid. Mechanical stops were built in to limit maximum displacements and a redundant leak-proof seal was added to minimize the chance of fluid escape.

The equivalent lumped mass model and its theoretical transfer function were determined from volume balance equations for the three chambers. Finite element models of the metal parts gave translational and volumetric spring rates. The fluid contributions taken into account were its bulk modulus and viscous loss in the damping chamber. The isolator was assumed to be massless for this model. The equivalent lumped mass model and its theoretical transfer function are shown in Figure 7. It may be seen from the transfer function that high frequency roll-off takes place with a slope of two rather than one as with a simple parallel spring and dashpot. Physically, this is because high frequency motion can be accommodated by volumetric changes in the chambers with no corresponding flow through the damping chamber and hence very low damping. The double peak in the transfer function occurs because with very low damping only  $k_1$  is effective whereas with very high damping  $k_1$  acts in parallel with the series combination of  $k_2$  and  $k_3$ . The PSD of axial acceleration at various force levels for the viscous isolator are shown in Figure 8. Both stiffness and damping are constant for the range of input considered. Transfer function tests down to the lowest threshold input attainable (.16  $\mu$  in.) indicated linear behavior. The damping properties of the isolator and the internal fluid pressure are a function of temperature. The pressure variation is controlled by the design of the thermal compensation bellows. A positive pressure margin is maintained to prevent

# Wire Rope Isolator PSD

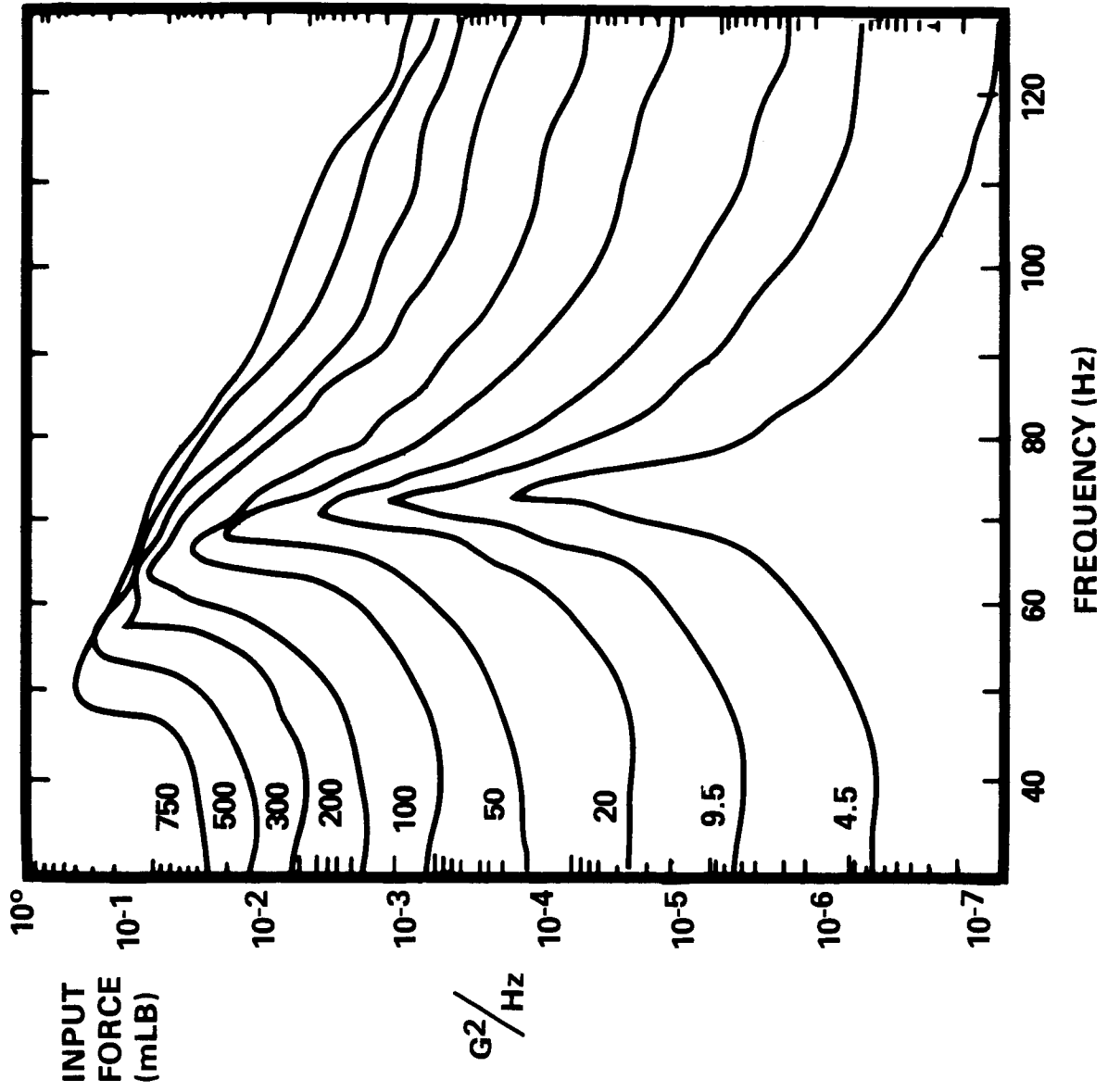


Figure 5



# Unit Isolator

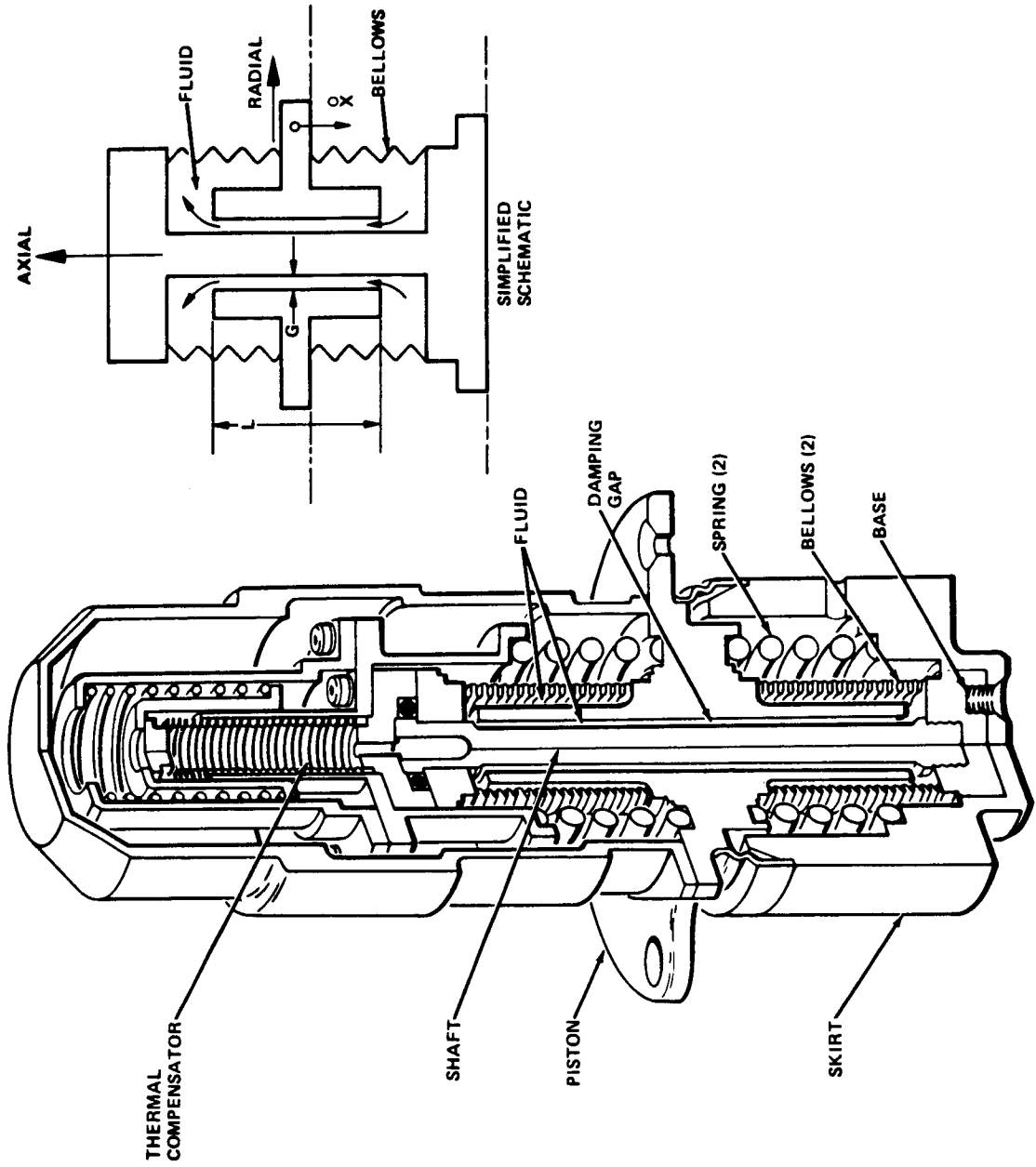
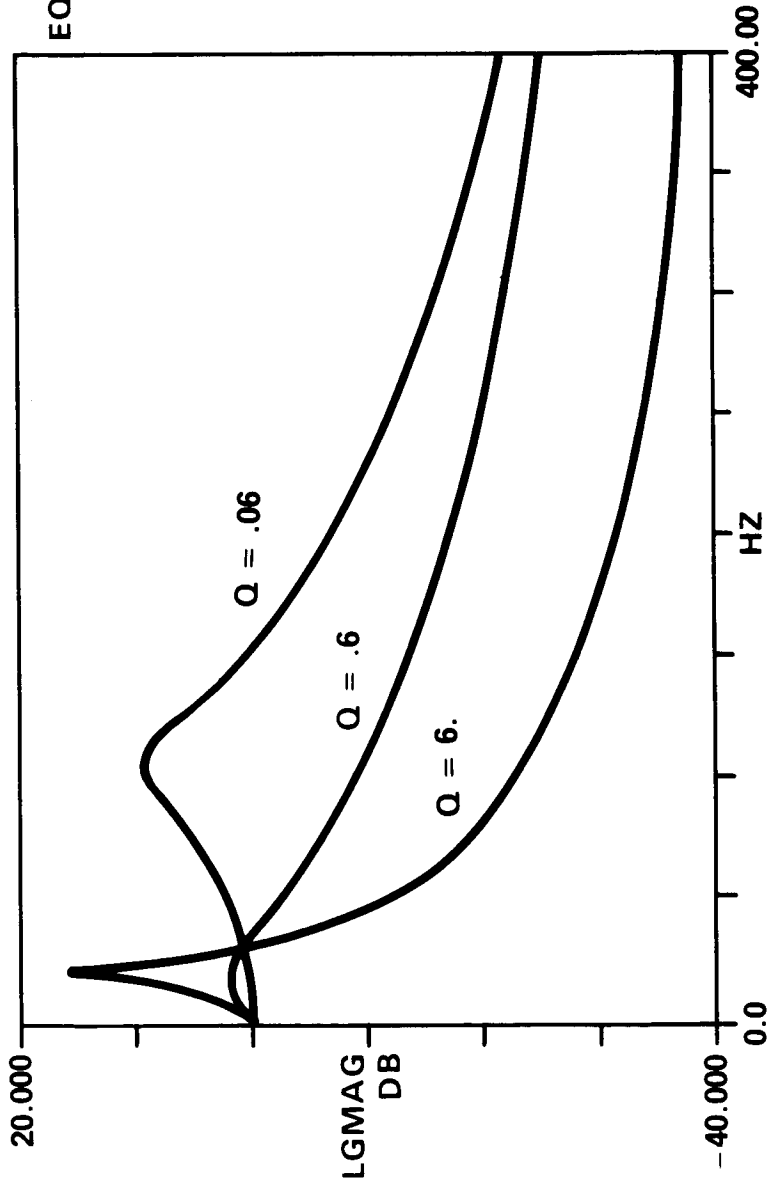


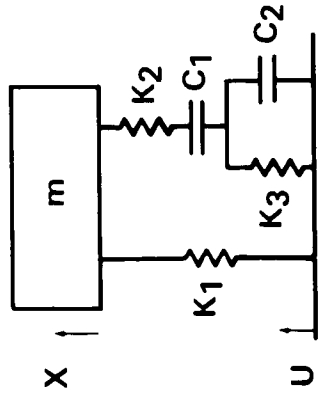
Figure 6

# Theoretical Isolator Transfer Function

$$T = \frac{1 + \left( \frac{MN + LN + M + N}{MNO} \right) \left( \frac{S}{P} \right) + \frac{L(N+1)}{NMQ^2} \left( \frac{S}{P} \right)^2}{1 + \left( \frac{MN + LN + M + N}{MNO} \right) \left( \frac{S}{P} \right) + \left( \frac{NMQ^2 + L(N+1)}{NMQ^2} \right) \left( \frac{S}{P} \right)^2 + \left( \frac{LN + M + N}{NMQ} \right) \left( \frac{S}{P} \right)^3 + \frac{L}{NMQ^2} \left( \frac{S}{P} \right)^4}$$



EQUIVALENT LUMPED MASS MODEL



- T = X/U
- N = K<sub>2</sub>/K<sub>1</sub>
- M = K<sub>3</sub>/K<sub>1</sub>
- L = C<sub>2</sub>/C<sub>1</sub>
- Q = √(K<sub>1</sub>m/c<sub>1</sub>)
- P = √(K<sub>1</sub>m/c<sub>1</sub>)

Figure 7



# Axial Displacement Power Spectral Density

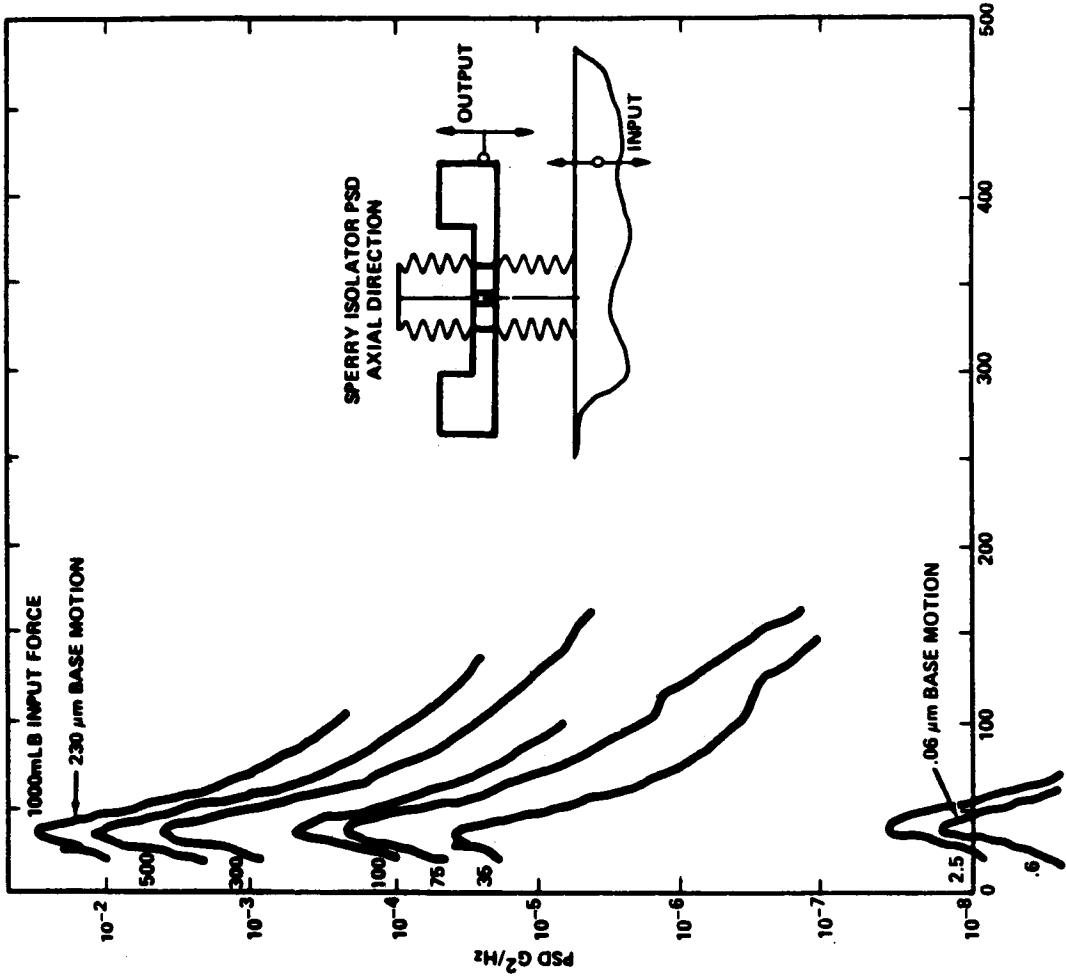


Figure 8

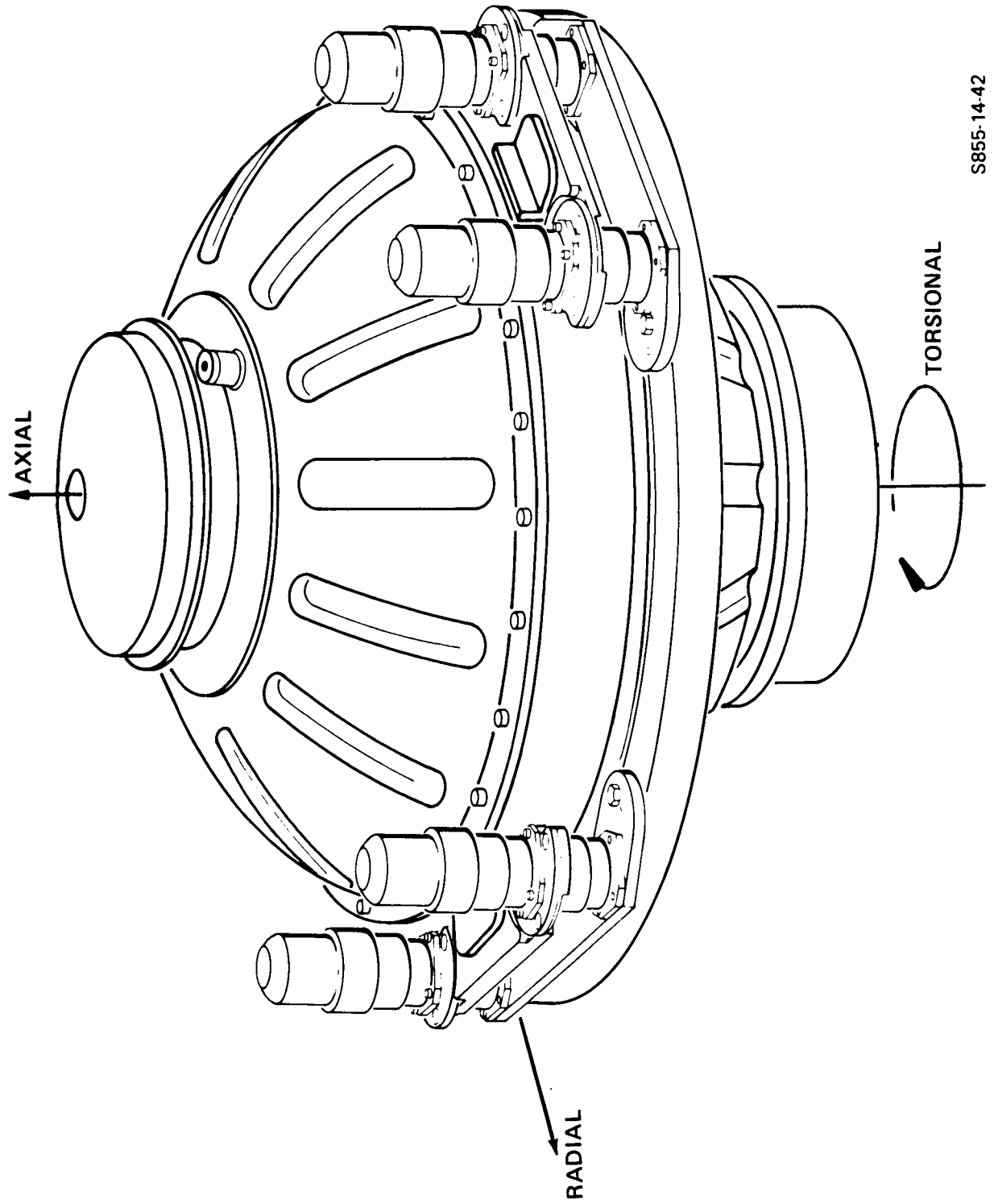
cavitation in the isolator. The variation in damping was deemed acceptable from a dynamic standpoint. An HST RWA mounted on an isolation system is shown in Figure 9. Three sets of two rigidly coupled isolator units are used to support the RWA at three points. For this application, the isolators are aligned for maximum damping in the axial direction. The structural attachments have been designed for on-orbit replacement of the isolation system, RWA, or RWA plus isolation system.

#### COMPONENT VIBRATION CHARACTERIZATION

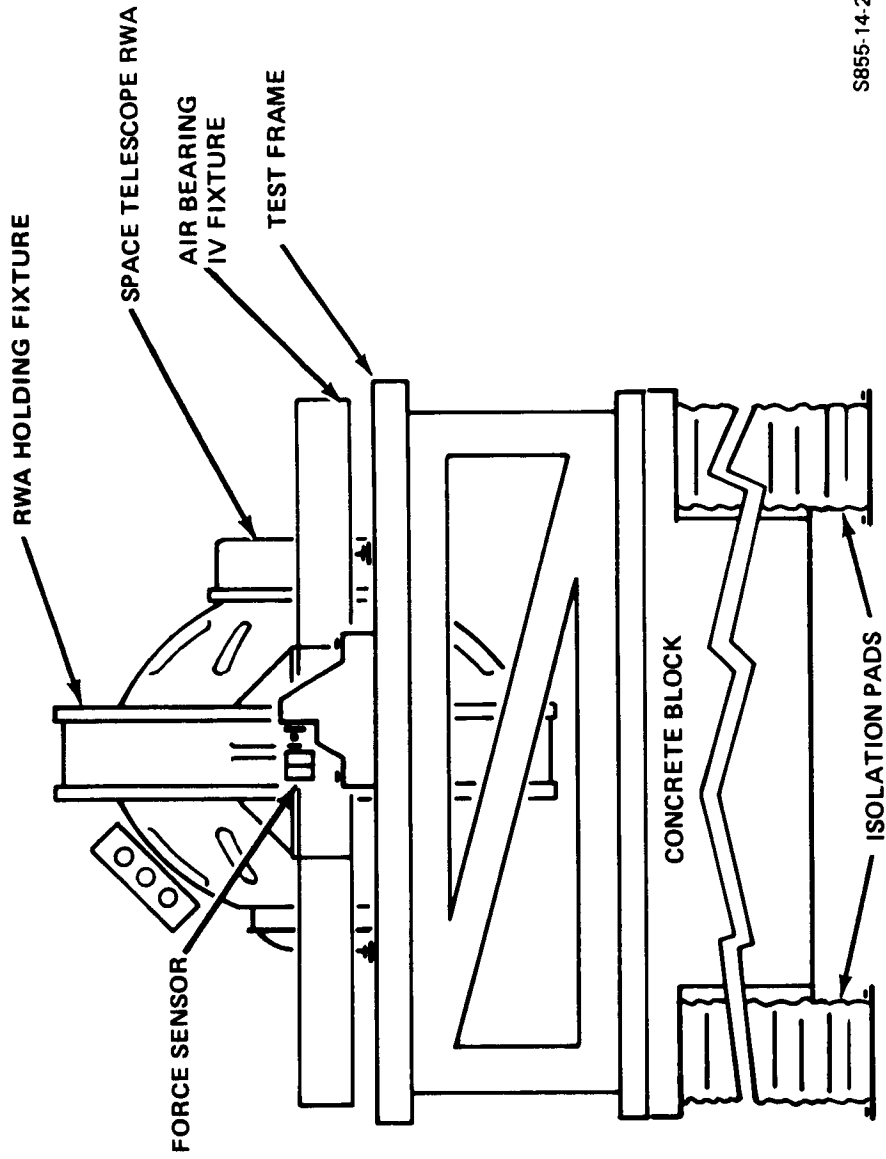
The test configuration for characterizing RWAs and isolation systems is shown in Figure 10. The RWA is mounted to a holding fixture through the isolators. The holding fixture is mounted to a large isolation mass through very stiff piezoelectric load cells. The holding fixture is supported by low friction gas bearings to ensure that the preponderance of force transmitted to the isolation block passes through the load cells. Summing networks permit measurements of forces and torques. The holding fixture can be rotated 90 degrees to measure axial or radial disturbances. Radial force measured during a wheel speed rundown without isolation is shown in Figure 11. This plot is a composite of force spectra taken at 16 second intervals during a 1600 second RWA rundown from 3000 rpm to zero wheel speed. The RWA was back-driven with constant torque so the wheel speed varied linearly. In the plot, harmonic disturbances occur at linearly varying frequencies whereas resonances in the RWA and test fixture occur at constant frequency. Peaking occurs where the two coincide. A resonance is evident around 105 Hz. A similar rundown plot for axial force is shown in Figure 12. The peak axial force recorded during the rundown was 3.390 pounds, when the 2X harmonic passed through a resonance at 80 Hz. An axial rundown with the wire rope isolators installed is given in Figure 13. Resonances from 20 to 50 Hz are present. The peak force recorded was .248 pound when the 1X harmonic passed through a resonance near 50 Hz. The ratios of these peaks are not a measure of the isolator attenuation but reflect the ratio of the Q of the RWA at its resonance to the Q of the isolator at its resonance, and also the square of the frequency ratio since force is proportional to speed squared. An axial rundown is plotted in Figure 14 for the Sperry viscous isolator with 200 centistoke damping fluid. An axial resonance lies at 20 Hz and a peak force of .053 pound was measured when the 1X harmonic crossed it. Again the ratio of the peak forces reflects the ratio of the Qs and speeds squared rather than isolator attenuation. When 350 centistoke fluid is used, the peak force is .025 pound. The difference in transmitted energy with and without isolation is dramatic. The LOS jitter predictions show a similar level of improvement with the isolation system.

The HST in dynamic test configuration is shown in Figure 15. It is suspended by three cables from air bags to simulate zero g conditions. The transfer function of vehicle angle response to control system torque was measured with RWAs isolated and nonisolated. The isolators did not alter the transfer characteristic. Figure 16 shows a close-up of the isolators in the test vehicle.

# RWA on Isolation System



# Induced Vibration Measurement System



S855.14.24

Figure 10

# HARD MOUNTED REACTION WHEEL RADIAL FORCE (.782 LB PEAK)

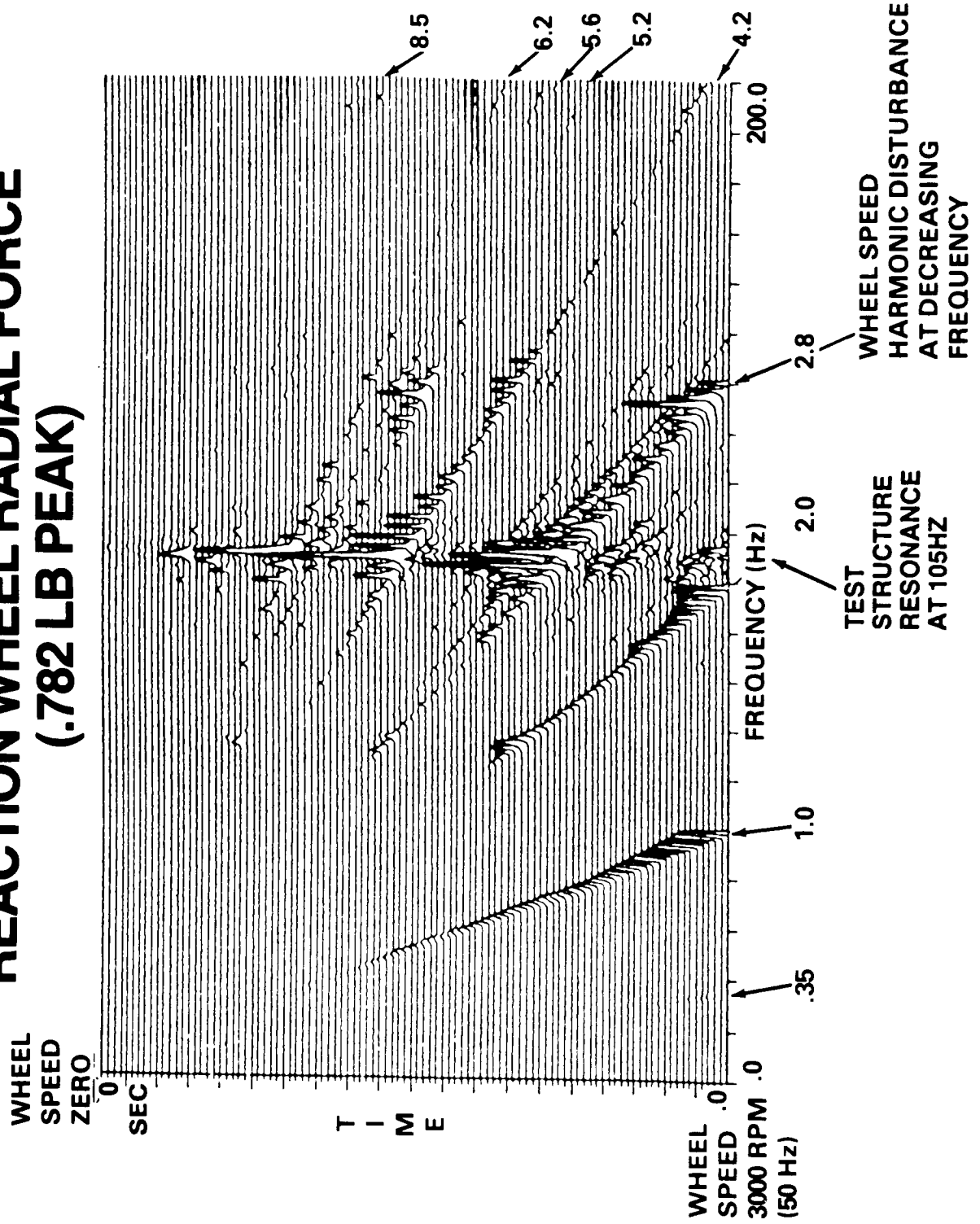
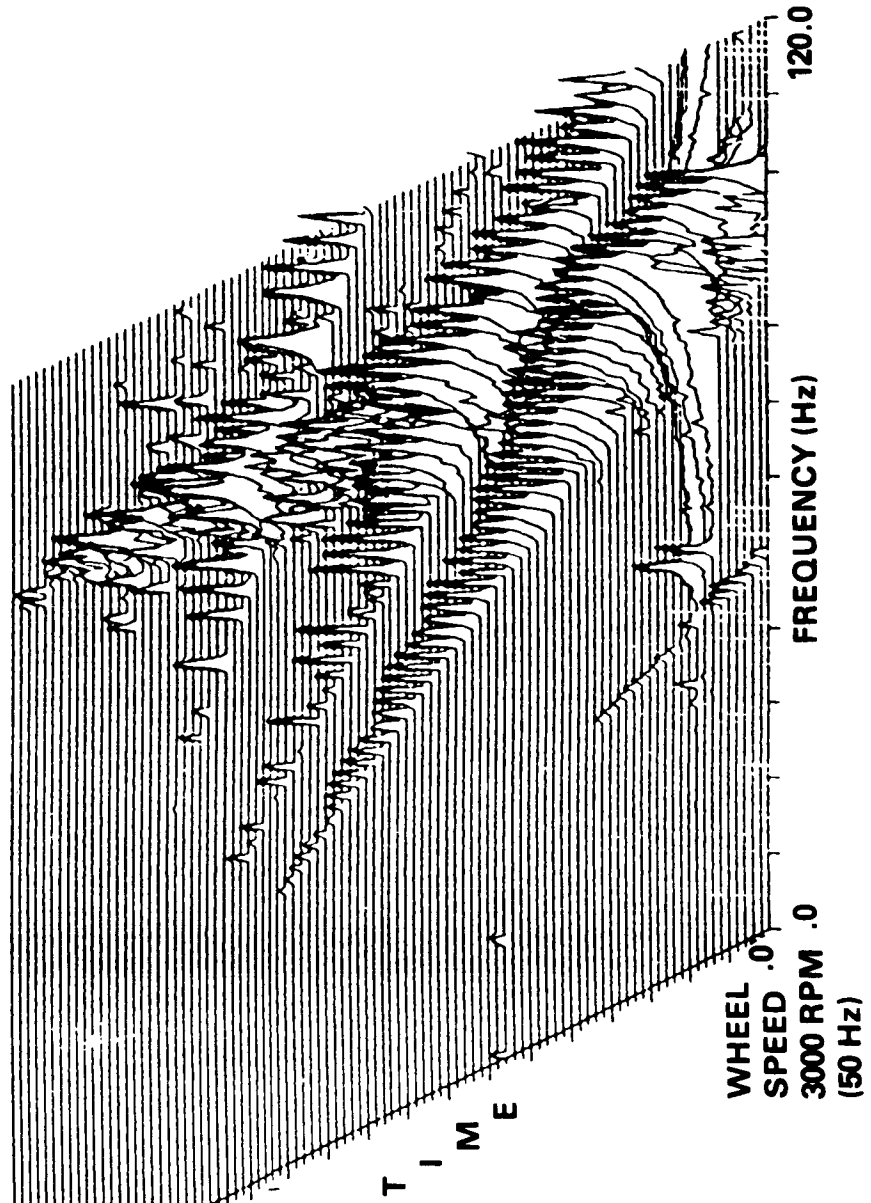


Figure 11

# HARD MOUNTED REACTION WHEEL AXIAL FORCE (3.39 LB PEAK)

WHEEL  
SPEED  
ZERO



ORIGINAL PAGE IS  
OF POOR QUALITY

Figure 12

**ISOLATED  
(WIRE ROPE ISOLATOR)  
REACTION WHEEL AXIAL FORCE  
(.284 LB PEAK)**

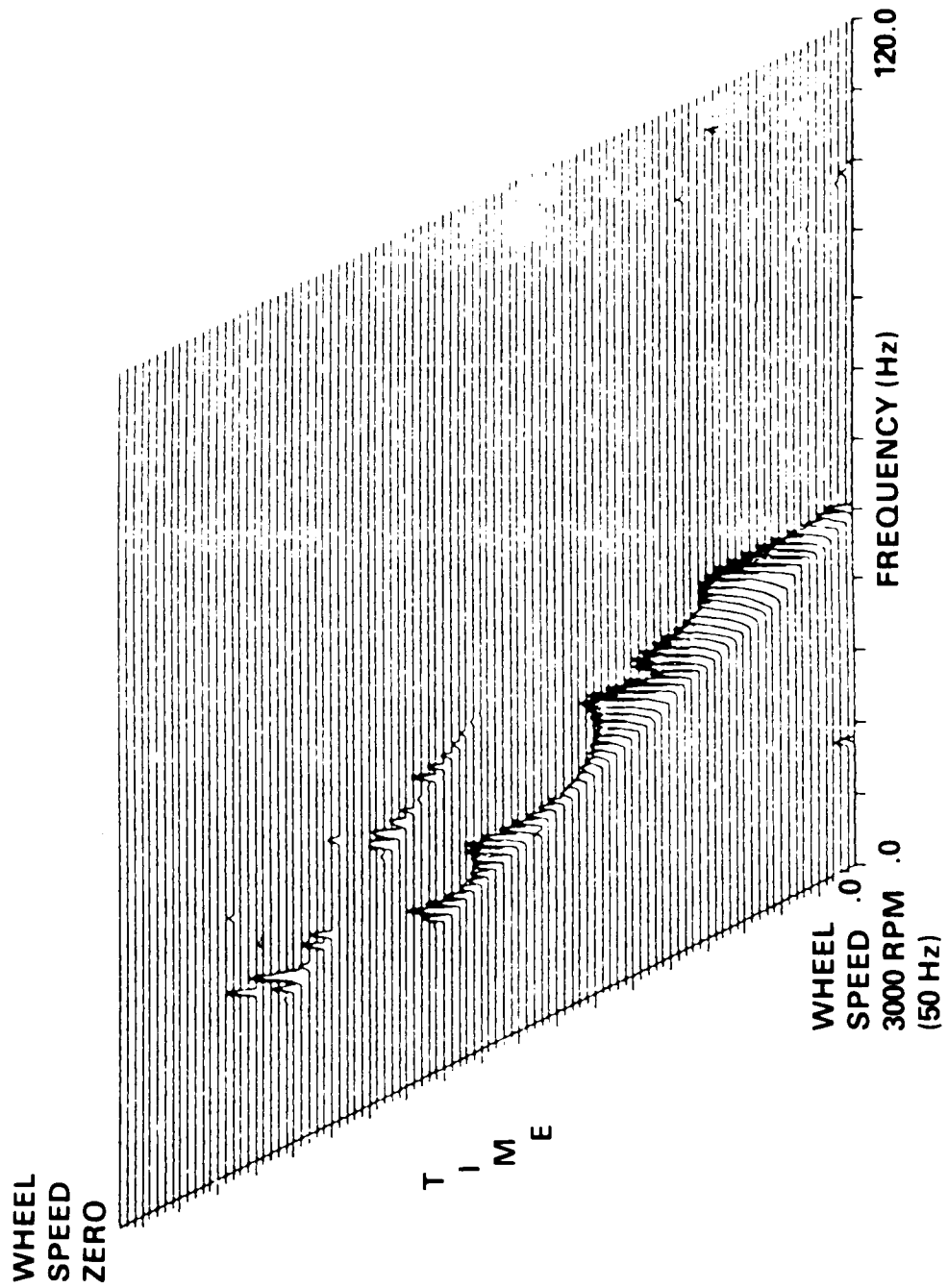
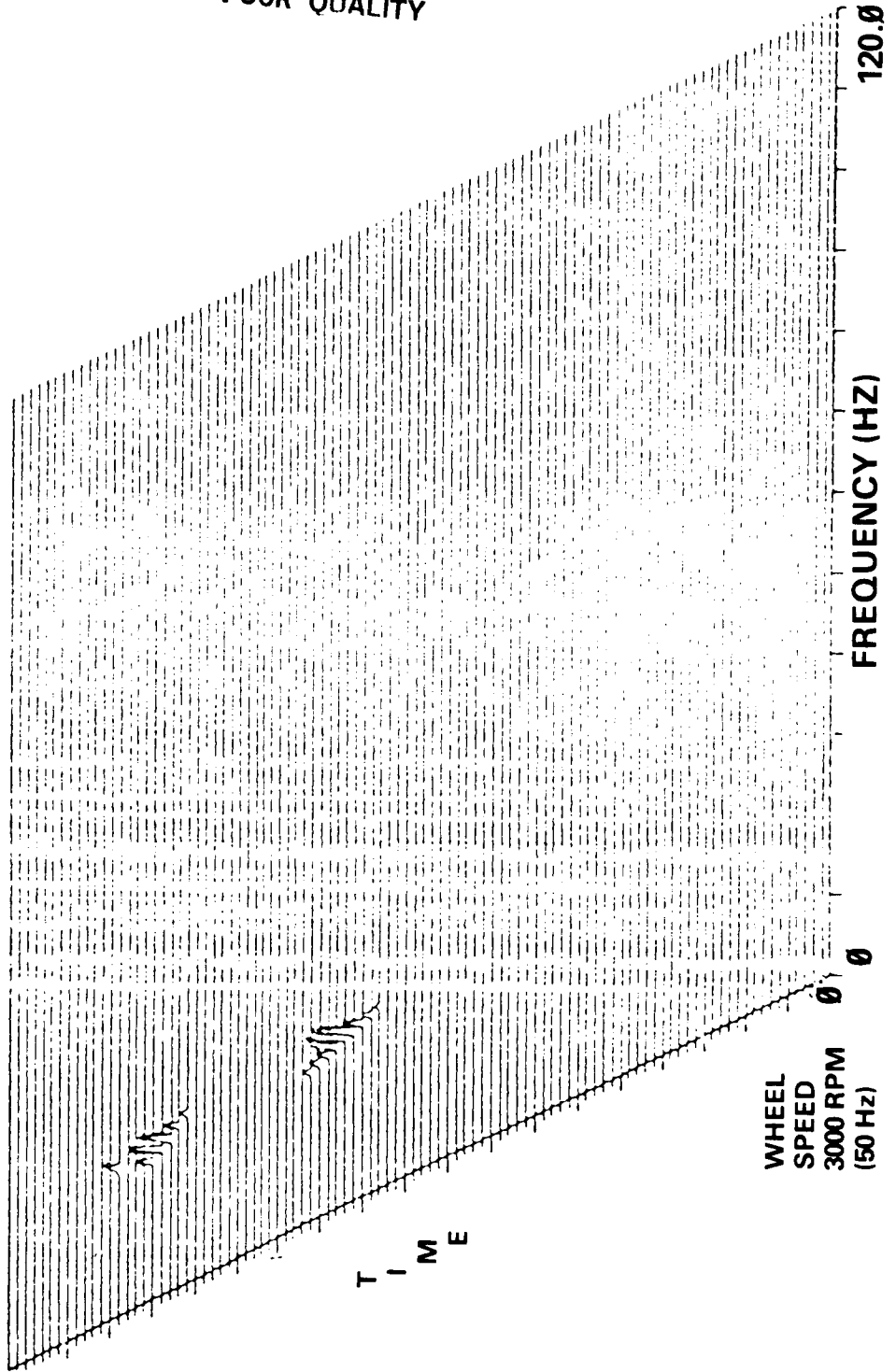


Figure 13

**ISOLATED  
(SPERRY VISCOUS ISOLATOR)  
REACTION SHEEL AXIAL FORCE  
(.052 LB PEAK)  
200 CS FLUID**

WHEEL  
SPEED  
ZERO



WHEEL  
SPEED  
3000 RPM  
(50 Hz)

ORIGINAL PAGE IS  
OF POOR QUALITY

Figure 14

## SUMMARY

The Hubble Space Telescope is a spacecraft with unique sensitivity to vibration disturbances. Its Reaction Wheel Assemblies cause coherent frequency disturbances in the millipound range. There are many harmonics of wheel speed and the disturbances are proportional to the square of wheel speed. A passive isolation system was developed to attenuate the higher frequency disturbances. The isolators utilize a metal spring in parallel with a viscous fluid damper, providing independent, deterministic control of the stiffness and damping characteristics. Second order roll-off of the transfer characteristic is obtained due to the volumetric spring rate of the isolator. Stiffness and damping were found constant over a disturbance amplitude range from  $.2 \times 10^{-6}$  to .04 inch of input amplitude. Damping is a function of temperature but for this application no compensation was required. The design has been space qualified and subjected to four times life fatigue testing. Component testing has demonstrated greater than two orders of magnitude reduction in peak axial force transmitted by an RWA. Ground testing has been conducted with the spacecraft suspended by cables from three air bags. Frequency response measurements of vehicle angle due to torque commanded have verified the flexibility of the isolators does not compromise the attitude control loop.

ORIGINAL PAGE IS  
OF POOR QUALITY

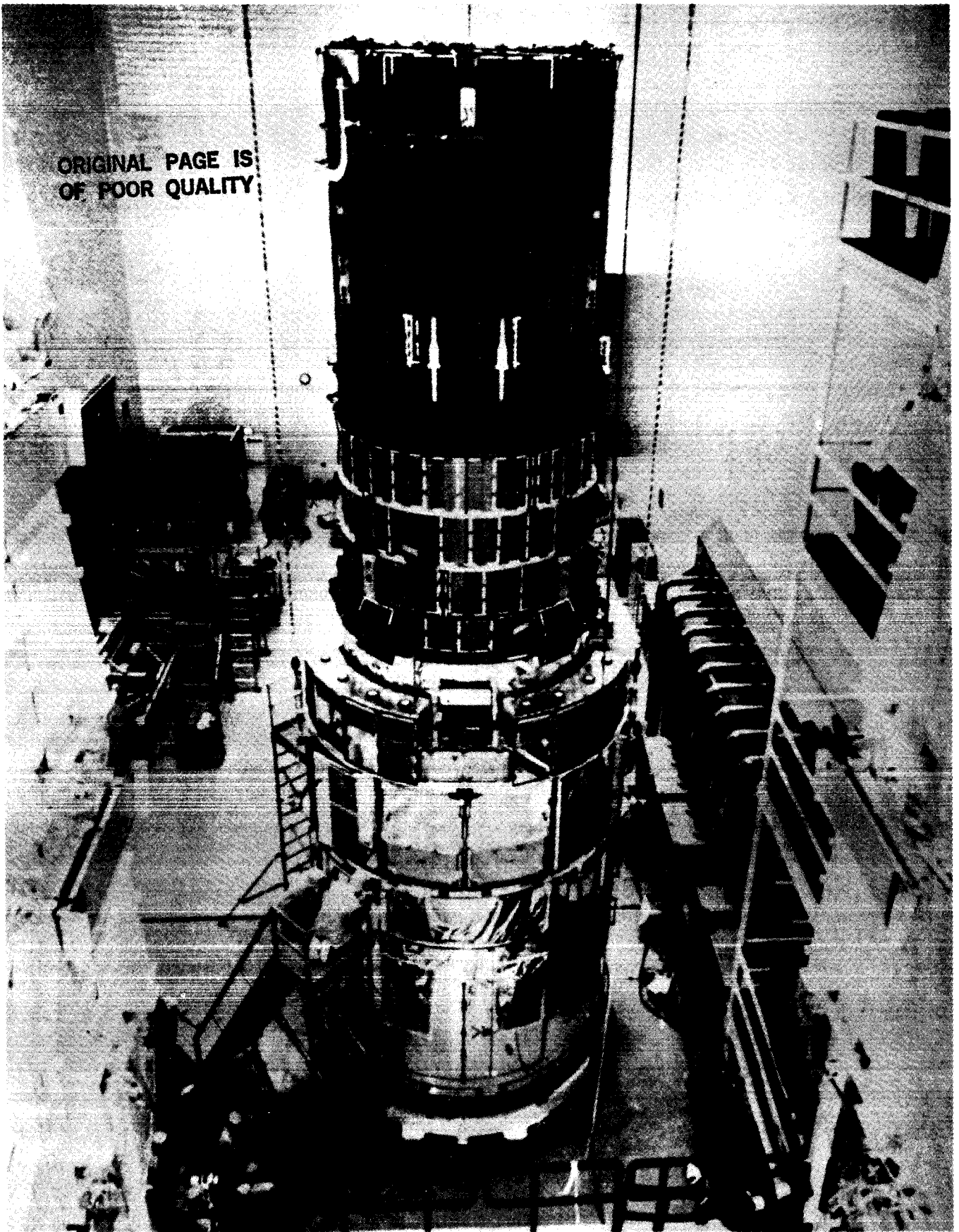


Figure 15

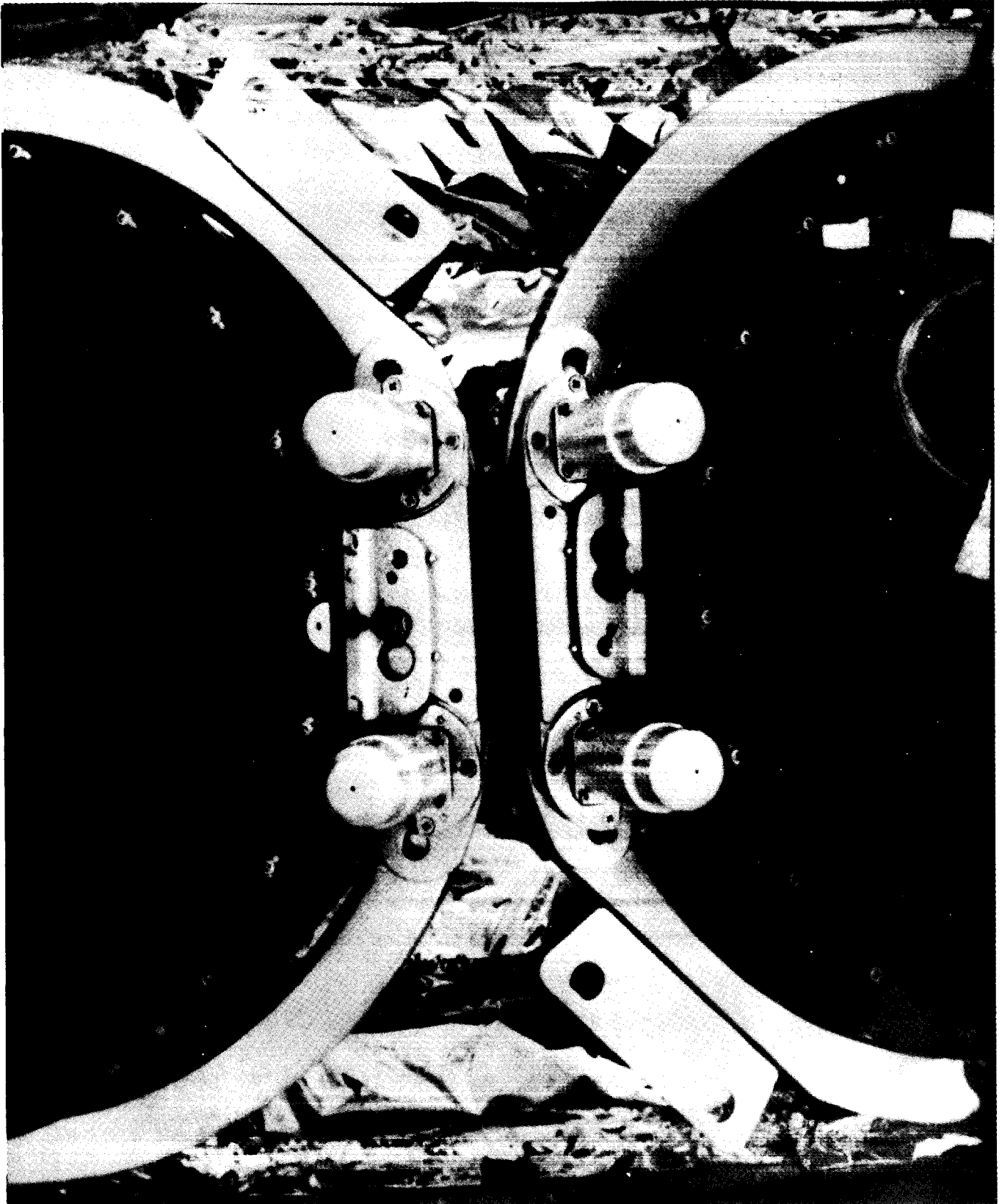


Figure 16

April 23, 1986 (Concurrent Sessions on Structures and Control)

Control Session 3A - George B. Doane, III, Chairman

Stiffness Control for Active Damping	J. L. Fanson and J. C. Chen, Jr.
A Quasi-Analytical Method for Non-Iterative Computation of Nonlinear Controls	J. L. Junkins and R. C. Thompson, Texas A&M; J. D. Turner, Cambridge Research
Decentralized Control of Large Space Structures via the GHR	D. K. Lindner, VPI
Control of Flexible Structures and the Research Community	J. S. Pyle and C. R. Keckler, LaRC

Control Session 3B - Robert Skelton, Chairman

Impact of Space Station Appendage Vibrations on the Pointing Performance of Gimballed Payloads	R. Hughes, GE
Maneuvering and Vibration Control of Flexible Spacecraft	L. Meirovitch and R. D. Quinn, VPI
Hubble Space Telescope Disturbances Caused by High Gain Antenna Motions	J. P. Sharkey, MSFC
Preliminary Evaluation of a Reaction Control System for the Space Station	H. H. Woo and J. Finley, RI/SD

This set of viewgraphs presents some of the results of research on control of flexible structures carried out at the California Institute of Technology and the Jet Propulsion Laboratory. This particular work has been underway since the fall of 1983. The research is supported by the JPL Director's Discretionary Fund, the NASA Graduate Student Researchers Program, and the NASA Office of Aeronautics and Space Technology. James Fanson is a graduate student in Applied Mechanics at Caltech, Thomas Caughey is Professor of Applied Mechanics at Caltech, and Jay-Chung Chen is a Member of the Technical Staff at the Jet Propulsion Laboratory.